

# Dielectric and piezoelectric properties of $\langle 001 \rangle$ fiber-textured $0.675\text{Pb}(\text{Mg}_{1/3}\text{Nb}_{2/3})\text{O}_3-0.325\text{PbTiO}_3$ ceramics

Edward M. Sabolsky,<sup>a)</sup> Susan Trolier-McKinstry, and Gary L. Messing  
*Materials Research Institute and Department of Materials Science and Engineering,  
 The Pennsylvania State University, University Park, Pennsylvania 16802*

(Received 18 October 2002; accepted 19 December 2002)

The  $0.675\text{Pb}(\text{Mg}_{1/3}\text{Nb}_{2/3})\text{O}_3-0.325\text{PbTiO}_3$  (PMN-32.5PT) ceramic composition (with 1 wt. % excess PbO) was fiber textured in the  $\langle 001 \rangle$  direction by the templated grain growth process using 5 vol % oriented  $\{001\}$ -BaTiO<sub>3</sub> platelet crystals as the templates. The templated ceramics annealed at 1150 °C for 5 h attained texture fractions as high as 0.9. The fiber-textured samples showed an increase in the piezoelectric, electromechanical coupling, and compliance coefficients when poled and measured in the  $\langle 001 \rangle$ -textured direction. The low drive field ( $< 5$  kV/cm)  $d_{33}$  coefficients in the  $\langle 001 \rangle$ , measured directly from unipolar strain-field measurements, were  $\sim 1150$  pC/N. This  $d_{33}$  coefficient is 1.2–1.5 times greater than randomly oriented samples. The poled  $\epsilon_{\text{max}}$  and  $\epsilon_{\text{rt}}$  for a 0.9-textured PMN-32.5PT ceramic were 21 500 and 2450, respectively. Factors limiting further property improvements are discussed. © 2003 American Institute of Physics.  
 [DOI: 10.1063/1.1554488]

## I. INTRODUCTION

$\langle 001 \rangle$ -oriented rhombohedral single crystal  $\text{Pb}(\text{Zn}_{1/3}\text{Nb}_{2/3})\text{O}_3-\text{PbTiO}_3$  (PZN-PT) and  $\text{Pb}(\text{Mg}_{1/3}\text{Nb}_{2/3})\text{O}_3-\text{PbTiO}_3$  (PMN-PT) near the morphotropic phase boundary (MPB) composition show enhanced strain levels combined with large piezoelectric and electromechanical coupling coefficients.<sup>1,2</sup> The large increase in these properties has been attributed to domain or crystallographic engineering. For single crystals poled in the  $\langle 001 \rangle$ , the dipoles are aligned along any of the four equivalent  $\langle 111 \rangle$  directions  $\sim 54.7^\circ$  from the poling direction. The four equivalent domains have the same energy state when the field is applied along the  $\langle 001 \rangle$ , which results in a low driving force for domain wall movement.<sup>1-3</sup> The limited mobility of the domain walls leads to the low observed piezoelectric (strain-field) hysteresis below the field-induced rhombohedral-tetragonal phase transformation. The enhanced strains are a result of the rotation of the dipoles towards the  $\langle 001 \rangle$  with increasing field. The macroscopic displacement during this phase transformation is pronounced for rhombohedral compositions very near to the MPB composition. The low hysteresis and high strain levels are desired for the next generation of piezoelectric actuators and transducers.

As previously stated, the enhanced electromechanical properties for the domain engineered materials have been primarily identified for PZN-PT and PMN-PT single crystals. Recently, BaTiO<sub>3</sub> and Zr-doped BaTiO<sub>3</sub> single crystals have shown similar increased properties and decreased piezoelectric hysteresis due to the application of the domain engineering concept for perovskite ferroelectrics which have a rhombohedral-tetragonal phase transition.<sup>4,5</sup> The domain engineering technique seems to be suitable for single crys-

tals, therefore, one would believe that domain engineering would also apply to thin films and grain-oriented ceramics in the  $\langle 001 \rangle$  of the same compositional systems. Regardless of the  $\langle 001 \rangle$  orientation of PMN-PT thin films, the piezoelectric coefficients always decrease as a result of substrate clamping.<sup>6,7</sup> The property enhancement due to  $\langle 001 \rangle$  grain orientation in rhombohedral, Pb-based relaxor-PbTiO<sub>3</sub> ceramics, or in any ferroelectric ceramic showing a rhombohedral-tetragonal MPB composition, has not yet been extensively investigated.

Many investigators have previously shown that ferroelectric ceramics which display a high degree of grain orientation (texture) possess directionally dependent dielectric, pyroelectric, and piezoelectric properties like those of a single crystal. This has been demonstrated for fiber-textured  $(\text{Sr},\text{Ba})\text{Nb}_2\text{O}_6$ ,<sup>8</sup>  $\text{PbNb}_2\text{O}_6$ ,<sup>9</sup> and  $\text{Bi}_4\text{Ti}_3\text{O}_{12}$ ,<sup>10,11</sup> PMN-32PT,<sup>12</sup> and sheet-textured  $(\text{Sr},\text{La})_2\text{Nb}_2\text{O}_7$ .<sup>13</sup> Duran *et al.*<sup>8</sup> showed that there was a direct correlation between the degree of fiber texture in the polar direction with the percentage of single crystal-like properties for  $(\text{Sr}_{0.53},\text{Ba}_{0.47})\text{Nb}_2\text{O}_6$  ceramics. As the degree of fiber texture increased in the  $[001]$ , the piezoelectric coefficient increased to a high fraction of the single crystal values. Therefore, by texturing ferroelectric ceramics by conventional ceramic processing routes, it is possible to obtain an inexpensive substitute for single crystals that display similar dielectric, pyroelectric, and piezoelectric properties. This is especially important for the PMN-PT composition since single crystal growth is limited by low production efficiency, high production cost, long growth time, small product size, limited shape forming capability, and compositional heterogeneity.

In this work,  $0.675\text{Pb}(\text{Mg}_{1/3}\text{Nb}_{2/3})\text{O}_3-0.325\text{PbTiO}_3$  (PMN-32.5PT) ceramics were fiber textured in the  $\langle 001 \rangle$  by the templated grain growth (TGG) process using a low concentration ( $\leq 5$  vol %) of oriented  $\{001\}$ -BaTiO<sub>3</sub> crystals as the template particles.<sup>12</sup> The TGG process involves the

<sup>a)</sup>Author to whom correspondence should be addressed; electronic mail: sabolsky@nextechmaterials.com

orientation of anisometric template particles in a fine-size powder by a shear-forming technique.<sup>14</sup> The template particles must be relatively large and anisometric in shape, so that they can be effectively oriented during forming and grow preferentially during sintering. The driving force for the TGG process is supplied by the difference in surface free energy between the templates and the matrix grains, which increases with the relative difference in the size between the templates and the matrix.

The objective of this work was to determine the effect of ⟨001⟩ fiber texture on the dielectric and piezoelectric properties of the PMN–32.5PT ceramics. Many issues are addressed in this work relating to the effect of excess PbO, residual BaTiO<sub>3</sub>, and texture degree on the piezoelectric response of the textured ceramics. The absence of three-dimensional texture and the presence of BaTiO<sub>3</sub> inclusions are two key issues which are addressed in this article, because they may have adverse effects on the piezoelectric response of the textured PMN–PT ceramics.

## II. EXPERIMENTAL PROCEDURE

The 0.675Pb(Mg<sub>1/3</sub>Nb<sub>2/3</sub>)O<sub>3</sub>–0.325PbTiO<sub>3</sub> (PMN–32.5PT) matrix powder used for the study was synthesized by the columbite method by milling MgNb<sub>2</sub>O<sub>6</sub> (TRS Inc., State College, PA), (PbCO<sub>3</sub>)<sub>2</sub>Pb(OH)<sub>2</sub> (Aldrich Chemical Company, Inc., Milwaukee, WI), and fumed-TiO<sub>2</sub> (Degussa-Hüs, Frankfurt, Germany) at the proper stoichiometry in deionized H<sub>2</sub>O (*pH* = 10.5). The composition was ball-milled for 12 h with high purity ZrO<sub>2</sub> media (3 mm diameter). The slurry was dried and the powder was reacted in an alumina crucible at 850 °C for 6 h. The average particle size of the PMN–32.5PT powder after milling, measured by centrifugal sedimentation (Horiba CAPA-700), was approximately 0.8 μm.

All textured samples characterized in this work contained 1 wt. % excess PbO in order to drive the TGG process to completion. The excess PbO was added by ball milling the proper concentration of (PbCO<sub>3</sub>)<sub>2</sub>Pb(OH)<sub>2</sub> with fully calcined PMN–32.5PT in toluene for 10 h. The powder was dried at ~100 °C and calcined at 550 °C for 4 h.

The matrix was mixed with 5 vol % {001}-BaTiO<sub>3</sub> template crystals which were grown by the Remeika process.<sup>15</sup> The template crystals displayed thicknesses of <75 μm and diameters of approximately 75–150 μm. The matrix composition was tape cast, cut, and laminated. The organic binder was first removed from the samples and the samples were then hot pressed in argon at 900 °C for 30 min at 40 MPa. The samples were cut to a dimension of 4 × 3 × 0.350 mm and annealed in O<sub>2</sub> at 1150 °C for times ≤5 h to allow adequate time for template growth to increase the total texture fraction. The sample densities were ~97% of theoretical density. The surface of the samples was polished to 1 μm roughness and x-ray diffraction (XRD) was performed on the sample surfaces to determine the texture fraction. The ⟨001⟩ texture fraction was estimated by the Lotgering method<sup>16</sup>

$$f_{(00l)} = \frac{P_{(00l)} - P_0}{1 - P_0}, \quad (1)$$

where

$$P_{(00l)} = \frac{\sum I_{(00l)}}{I_{(hkl)}}, \quad (2)$$

$$P_0 = \frac{\sum I_{0(00l)}}{I_{0(hkl)}}. \quad (3)$$

$\sum I_{(00l)}$  is the summation of the XRD peak intensities of all the (00l) peaks (i.e., 001, 002...) in the textured sample pattern.  $\sum I_{(hkl)}$  is the summation of the peak intensities of all (hkl) peaks which appear in the XRD pattern.  $\sum I_{0(00l)}$  and  $\sum I_{0(hkl)}$  are summations of the XRD peak intensities for a randomly oriented sample. The *f* factors were calculated for a 2θ scan between 20° and 70°. The calculated *f* describes the degree of texture defined by the surface area which was characterized by XRD. The *f* factor is considered to be an estimation of the volume fraction of textured material. The texture fractions varied across the volume of the samples due to the size and inhomogeneous mixing of the large template particles. The texture fractions reported for each sample in this work were calculated and averaged over ≥3 XRD patterns taken at various depths through the sample thickness. The listed texture fractions are accurate to ±5%, therefore, the samples displaying similar texture fractions, which were similar within ±5%, were grouped for property versus texture comparisons.

Randomly oriented, untemplated samples of the various matrix compositions (with 0 wt. % and 1 wt. % excess PbO) were formed in order to directly correlate the effect of processing on the properties. Throughout this work, the term “random” will designate PMN–32.5PT samples that do not contain BaTiO<sub>3</sub> template particles and the samples display no preferential grain orientation. The random pellet samples were formed by isostatic pressing at room temperature. The random samples were sintered at 1150 °C and then polished to a final dimension of ~6.3 mm in diameter and 0.350 mm in thickness. These sample dimensions were chosen in order to have untextured/untemplated samples with a similar area and thickness as the textured samples. The sample densities were ~98%–99% of theoretical density, depending upon the excess PbO content. Samples that lost >0.5 wt. % after sintering were discarded from the study.

The low-field dielectric constant and loss (at 1 V) were measured as a function of temperature with a multifrequency impedance meter (HP 4284A LCR meter) combined with a temperature regulated oven. The dielectric constant and loss were measured between 0 and 300 °C and over a frequency range of 1 kHz–1 MHz. Poled samples were measured on heating and unpoled samples were measured on cooling. The samples were heated and cooled at a rate of 4 °C/min. The untextured and textured PMN–32.5PT samples were typically poled with a dc bias of 40 kV/cm for 15 min at room temperature in polydimethylsiloxane (Dow Corning 200 fluid). The samples were electroded with gold by sputtering.

The dielectric polarization versus electric field measurements (*P*–*E* hysteresis loops) were completed using a modified Sawyer–Tower circuit. The unipolar strain versus electric field measurements (strain–field curves) were concurrently measured using the Sawyer–Tower circuit in

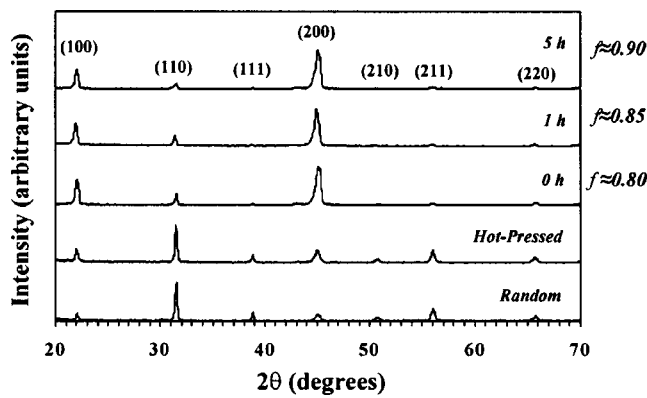


FIG. 1. XRD pattern of PMN-32.5PT (1 wt. % excess PbO) ceramics containing 5 vol % oriented {001}-BaTiO<sub>3</sub> templates annealed at 1150 °C for 0–5 h.

conjunction with a linear variable differential transducer, driven by a lock-in amplifier (Stanford Research Systems, Model SR830). High fields were generated by a Trek 609C-6 high-voltage amplifier. The strain and polarization of the samples were measured while immersed in Galden HT-200 to prevent arcing. The  $P$ - $E$  measurements were traced using a triangular wave form. Unipolar strain-field curves were measured using the same apparatus by applying half of a sinusoidal wave to the poled samples.

The low-field piezoelectric coefficients ( $d_{33}$ ) for the samples were estimated from the slope of the unipolar strain-field curves. The longitudinal and lateral electromechanical coupling coefficients ( $k_{33}, k_{31}$ ) were measured in accordance with the IEEE standards for the resonance technique (ANSI/IEEE Std. 176-1978)<sup>17</sup> using a HP 4194A impedance/gain phase analyzer. From the measured resonance  $f_r$  and antiresonance  $f_a$  frequencies, the compliance ( $s_{33}^E, s_{33}^D, s_{11}^E, s_{11}^D$ ) and piezoelectric coefficients ( $d_{33}, d_{31}$ ) were also calculated. The  $f_r$  and  $f_a$  frequencies were determined from the first minimum and maximum impedance peaks in the impedance/frequency scan.

### III. RESULTS AND DISCUSSION

#### A. Textured PMN-32.5PT ceramics

Figure 1 shows the evolution of the XRD patterns for PMN-32.5PT ceramics with a matrix containing 5 vol % BaTiO<sub>3</sub> templates (PMN-32.5PT-5BT) and 1 wt. % excess PbO annealed at 1150 °C for 0–5 h. The samples were initially densified by hot pressing as described in the experimental procedures. Included in Fig. 1 are the XRD patterns of a random PMN-32.5PT and an unannealed PMN-32.5PT-5BT ceramic sample. Figure 1 shows no alteration in the XRD pattern of the templated sample after hot pressing compared to that for the random sample. The additional oriented template particles did not appear to affect the relative intensities due to the increased volume fraction of oriented material within the ceramic. When the templated samples were heated at a rate of 10 °C/min to 1150 °C and then quenched to room temperature (0 h anneal), the peak intensity of the {001} increased and all other peaks decreased in intensity. A Lotgering factor of  $\sim 0.8$  was calculated for

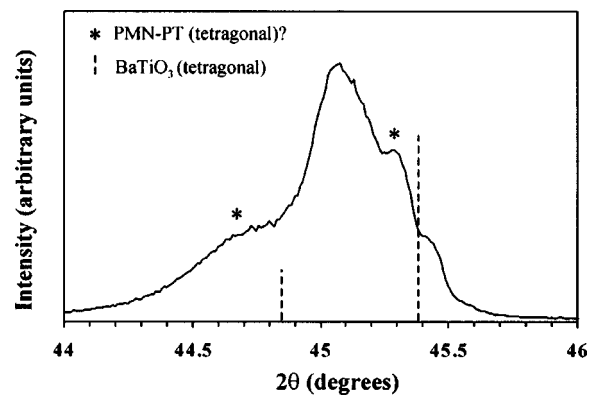


FIG. 2. XRD pattern of the (200) peak of a  $\sim 90\%$ -textured PMN-32.5PT (1 wt. % excess PbO) ceramic containing 5 vol % oriented {001}-BaTiO<sub>3</sub> templates annealed at 1150 °C for 5 h.

these samples. This indicates that a significant amount of template growth occurred just on heating to 1150 °C. With annealing at 1150 °C for 1 and 5 h, the texture fraction increased to  $\sim 0.85$  and  $0.90$ , respectively (Fig. 1). These results indicate that the texture rate seemed to begin saturating before the sample reached the 1150 °C annealing temperature. The saturation of the texturing rate can be attributed in part to the decrease in the growth rate of the oriented PMN-PT single crystal layers heteroepitaxially growing from the BaTiO<sub>3</sub> templates due to the coarsening and shape change of the matrix grains, as previously reported.<sup>18</sup> A second factor slowing the rate of texturing is the impingement of the templated grains, since the template particles are not ideally situated in the ceramic.

An interesting feature that can be observed in the XRD patterns (Fig. 1) for the textured samples is the broad {001} peaks, where these peaks sometimes display multiple overlapping peaks in close proximity of the  $2\theta$  angle position. The peak splitting is only observed for the {001} peaks. Therefore, the origin of the splitting is related to the templated grains since the increased intensity of these peaks is based primarily on the diffraction from the oriented grains. Figure 2 shows an XRD step scan around the (200) diffraction peak for a 90%-textured PMN-32.5PT-5BT ceramic. The BaTiO<sub>3</sub> peak positions are shown for reference. It is clear that the splitting of the {200} peaks does not overlap with the rhombohedral PMN-PT peaks or the (200)/(002) peaks of tetragonally distorted BaTiO<sub>3</sub>. The multiple peaks could be the result of lattice distortions in the templated grains due to interdiffusion between the template and the growing crystal layer. The templated PMN-32.5PT grains may also be mechanically constrained by the BaTiO<sub>3</sub> template which may locally lock the grown PMN-PT crystal into the tetragonal phase. Durbin *et al.*<sup>19</sup> recently showed the coexistence of rhombohedral and tetragonal domains in poled PZN-8PT single crystals (a rhombohedral composition) by XRD of the {002} peak. The appearance of Fig. 2 (at  $2\theta > 44.8^\circ$ ) is similar to that shown by Durbin *et al.* The PMN-32.5PT composition is an analogous composition to the PZN-8PT composition in relation to the MPB. Therefore, the splitting in the diffraction pattern may indicate that

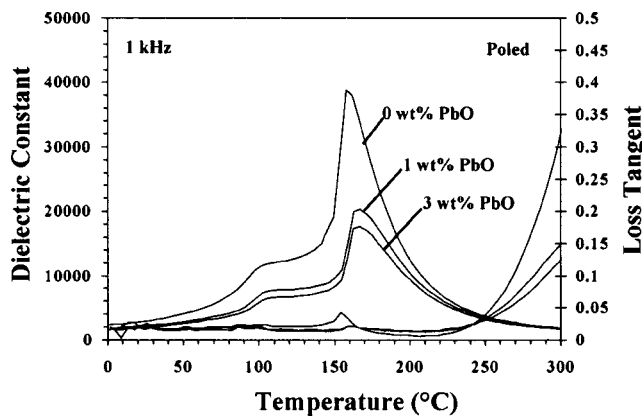


FIG. 3. Dielectric constant and loss as a function of temperature for poled PMN-32.5PT ceramics containing 0, 1, and 3 wt. % excess PbO.

the BaTiO<sub>3</sub> templates are stabilizing the tetragonal domain structure in the templated grains by clamping.

### B. Dielectric properties of <001>-textured PMN-32.5PT ceramics

As previously mentioned, all templated samples in this work contained 1 wt. % excess PbO in order to enhance the grain growth kinetics. The effect of an intergranular Pb-rich phase on the dielectric properties of PMN-PT has been reported by many authors.<sup>20-28</sup> The thin, intergranular layer of a Pb-rich phase lowers the dielectric constant and increases the loss for various PMN-PT compositions. These effects have been successfully described by brick-wall dielectric mixing laws.<sup>20-28</sup>

A comparison of the dielectric constants and loss tangents versus temperature for poled, random PMN-32.5PT ceramic samples containing 0, 1, and 3 wt. % excess PbO is displayed in Fig. 3. The poled samples display two major anomalies in the dielectric constant as a function of temperature. The anomaly at ~90–100 °C ( $T_{r-t}$ ) indicates the phase transition from the ferroelectric rhombohedral to the tetragonal state.<sup>29-31</sup> The second anomaly describes the phase transition from the ferroelectric tetragonal state to the paraelectric cubic state.<sup>29-34</sup> The ferroelectric tetragonal to paraelectric cubic transition temperature will be designated as the maxima temperature  $T_{max}$ , since the PMN-32.5PT composition shows a slightly broad phase transition. PMN-PT compositions containing lower PbTiO<sub>3</sub> concentrations usually show greater dielectric broadening at the paraelectric-ferroelectric phase transition due to compositional fluctuations.<sup>29,30,32,33</sup> The broad phase transition indicates the presence of multiple localized phase transition temperatures, therefore the dielectric anomaly maximum is usually termed the  $T_{max}$ .  $T_{max}$  for the random PMN-32.5PT ceramic containing 0 wt. % excess PbO was 159 °C. The phase diagram reported by Zhao *et al.*<sup>31</sup> shows that a PMN-PT composition with 32.5 mol % PbTiO<sub>3</sub> has a  $T_{max} \approx 162$  °C and a  $T_{r-t} \approx 78$  °C. This implies that the actual matrix composition for this study may be between 31.5 and 32 mol % PbTiO<sub>3</sub>, since the MPB of the PMN-PT system curves toward the PMN composition resulting in a higher  $T_{max}$  and a lower  $T_{r-t}$ .

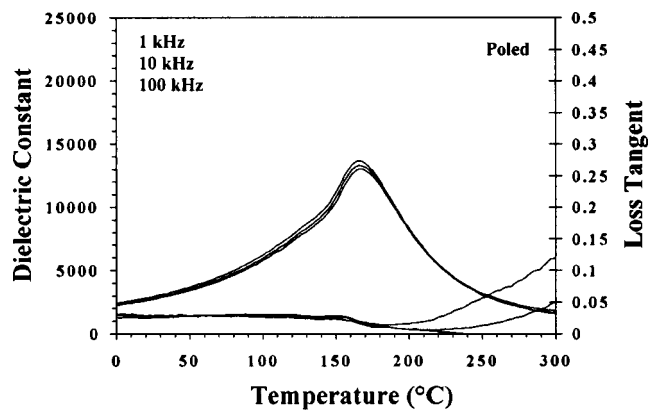


FIG. 4. Dielectric constant and loss as a function of temperature for poled PMN-32.5PT ceramics containing 5 vol % BaTiO<sub>3</sub> templates (PMN-32.5PT-5BT) annealed at 800 °C for 10 h.

With the addition of 1 wt or 3 wt. % excess PbO, the poled  $\epsilon_{max}$  decreased from ~39 000 to ~20 300 and ~17 700 (1 kHz), respectively (Fig. 3). The addition of excess PbO also shifted the phase transition temperatures ( $T_{r-t}$ ,  $T_{max}$ ) to higher temperatures. The  $T_{max}$  was shifted from 159 to ~167 °C with the addition of 1–3 wt. % excess PbO. Shifts in the  $T_{max}$  for PMN and PZT have been attributed to the volume of intergranular low- $\epsilon$  (low polarizable) phases and defects.<sup>26,35</sup> The presence of low- $\epsilon$  phases and vacancies at the grain boundaries affects the space-charge field and surface stresses around the grains. The presence of intergranular imperfections may alter the stress distribution and stabilize the space-charge field around the grains which would “lock-in” the ferroelectric polarization, allowing the dipoles to persist to higher than normal temperatures.<sup>26,35,36</sup> The dielectric loss for these samples containing excess PbO was still relatively low ( $\delta < 0.05$ ).

Figures 4 and 5 show plots of the dielectric constant as a function of temperature for PMN-32.5PT ceramic samples containing 5 vol % {001}-BaTiO<sub>3</sub> template particles (PMN-32.5PT-5BT). The samples all contained 1 wt. % excess PbO in order to increase the TGG kinetics. The samples were densified to ~99% by hot pressing in argon. Each sample experienced a different high temperature annealing treatment

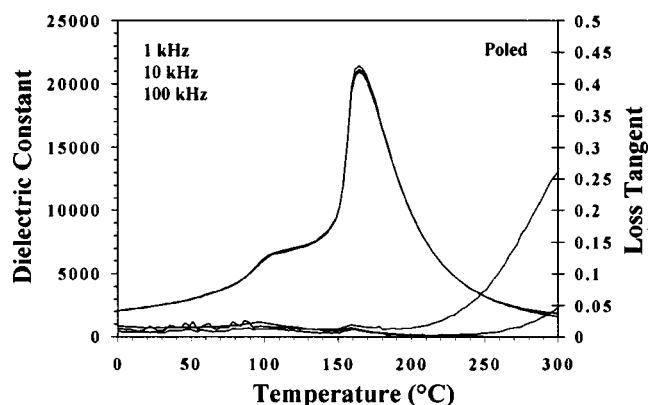


FIG. 5. Dielectric constant and loss as a function of temperature for poled PMN-32.5PT ceramics containing 5 vol % BaTiO<sub>3</sub> templates (PMN-32.5PT-5BT) annealed at 1150 °C for 5 h.

to drive the TGG process. The first sample set was only annealed to 800 °C for 10 h in order to reoxidize the sample without altering the untextured ( $f \approx 0$ ) PMN-PT/BaTiO<sub>3</sub> microstructure (Fig. 1). The second sample was annealed to 1150 °C for 5 h, which resulted in the sample having a  $\langle 001 \rangle$ -texture fraction of  $\sim 0.90$  (Fig. 1). The poled dielectric response of the untextured PMN-32.5PT-5BT sample (Fig. 4) showed a broad peak at  $T_{\max} \approx 167$  °C. This untextured PMN-32.5PT-5BT sample displayed a more diffuse transition than the random samples, possibly due to differences in point defects, grain size, or internal stresses. The rhombohedral-tetragonal transition at  $T_{r-t}$  ( $\sim 95$ – $105$  °C for random 1 wt. % excess PbO samples) could not be identified. The  $T_{\max}$  ( $\sim 163$  °C) was not affected by the addition of the BaTiO<sub>3</sub> templates. This indicates that little Ba homogenization (i.e., solid solution formation) occurs at this temperature and time.<sup>37–41</sup> The hot-pressed PMN-32.5PT-5BT ceramic showed a lower  $\epsilon_{\max}$  ( $\sim 14\,460$  at 1 kHz). By utilizing dielectric series and logarithmic mixing laws, it was predicted that a 5 vol % BaTiO<sub>3</sub> addition to PMN-32.5PT (1 wt. % excess PbO) ceramic would cause a decrease of  $< 2100$  in the effective dielectric constant.<sup>20,21,26</sup> Therefore, the addition of the BaTiO<sub>3</sub> phase could not account completely for the decrease in the dielectric response. Chu *et al.* reported that Pb vacancies in Pb(Sc<sub>1/2</sub>Nb<sub>1/2</sub>)O<sub>3</sub> (PSN) ceramics resulted in a decrease in the transition temperature and dielectric constant.<sup>42</sup> The Pb vacancies were reported to inhibit dipole coupling and broaden the ferroelectric transformation. The presence of Pb vacancies in the PMN-PT templated samples after hot pressing and the annealing treatment may have influenced the dielectric behavior in a similar manner. Also, the presence of large grains and possible residual stresses could partially account for this decrease.

With an increase in texture fraction to  $\sim 0.90$  for higher processing temperatures (1150 °C, 5 h), the diffuseness of the permittivity peak decreased and the overall constant increased, especially at  $T_{\max}$  (Fig. 5).  $T_{\max}$  did not change, remaining at a temperature of  $\sim 164$  °C. The rhombohedral-tetragonal transition was visible in the dielectric data for the poled sample (Fig. 5), and the transition temperature was consistent with that of that of the random, BaTiO<sub>3</sub>-free samples ( $T_{r-t} \approx 95$ – $105$  °C). The stability of the transition temperatures indicates that the BaTiO<sub>3</sub> templates remained stable within the PMN-PT matrix without the formation of a solid solution between the two phases.<sup>37–41</sup> The increase in the dielectric constant may have been influenced by the high temperature processing which could have eliminated Pb and oxygen vacancies or residual stresses in the ceramic after hot pressing in addition to the large grain size.<sup>42</sup> While the dielectric constant values increased with an increase in texture fraction, the maximum permittivity was still dominated by the presence of the intergranular low- $\epsilon$  phase.

The stability of the transition temperatures for the PMN-32.5PT-5BT samples suggested the high stability of the BaTiO<sub>3</sub> templates. Since the BaTiO<sub>3</sub> did not seem to diffuse into the matrix, then the apparent increase in the transition breadth cannot be attributed to dissolution, as reported for PMN and PZN solid solutions.<sup>37,40,43</sup> Some of the broadening of the dielectric peak can be attributed to the presence

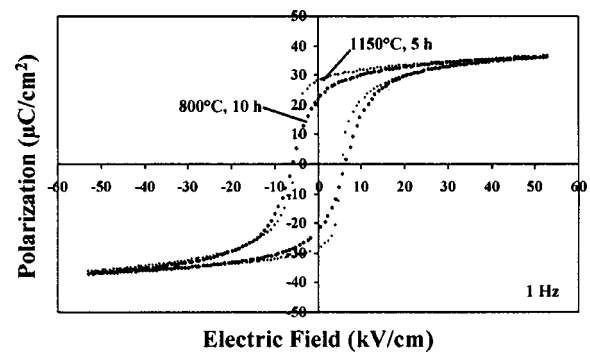


FIG. 6. Polarization-electric field hysteresis for PMN-32.5PT ceramic containing 5 vol % BaTiO<sub>3</sub> templates (PMN-32.5PT-5BT) annealed at 800 °C for 10 h and 1150 °C for 5 h.

of intergranular PbO acting as a Curie point depressor.<sup>24</sup> The diffuse transition can also be related to the possible distribution of space charge in the material. Space charge may also develop along the grain boundaries due to the intergranular low- $\epsilon$  phase.<sup>26,27</sup> Therefore, the decrease in diffuseness may not be the result of texturing, but a result of the high temperature annealing.<sup>26,27,42</sup> Another contribution to the diffuseness may be the combined contributions of both the BaTiO<sub>3</sub> and the PMN-PT, which have transition temperatures that are  $\sim 40$ – $50$  °C apart.

### C. Ferroelectric hysteresis of $\langle 001 \rangle$ -textured PMN-32.5PT ceramics

The dielectric polarization as a function of bipolar electric field measured in the textured  $\langle 001 \rangle$  for the PMN-32.5PT-5BT is displayed in Fig. 6. Again, the one PMN-32.5PT-5BT sample was only annealed to 800 °C for 10 h in order to reoxidize the sample without altering the untextured ( $f \approx 0$ ) PMN-PT/BaTiO<sub>3</sub> microstructure. The other sample was annealed to 1150 °C for 5 h resulting in a texture fraction of  $\sim 0.9$ . The maximum saturation polarization for the PMN-32.5PT-5BT composition was similar for both the untextured and textured PMN-32.5PT-5BT samples, although the loop was more square in the textured materials. The untextured PMN-32.5PT-5BT composition showed a  $P_r \approx 22$   $\mu\text{C}/\text{cm}^2$  and  $E_c \approx 5.9$  kV/cm. With an increase of texture fraction, the polarization increased and the coercive field remained relatively unchanged ( $P_r \approx 28$   $\mu\text{C}/\text{cm}^2$ ,  $E_c \approx 5.6$  kV/cm). The coercive field for the highly textured sample was similar to a random PMN-32.5PT ( $E_c \approx 5.1$  kV/cm) and lower than a random ceramic containing 1 wt. % excess PbO ( $E_c \approx 6.7$  kV/cm). The remanent polarization of the highly textured sample was lower than that displayed by random PMN-32.5PT samples ( $P_r \approx 35$   $\mu\text{C}/\text{cm}^2$  for 0 wt. % excess PbO and  $P_r \approx 32$   $\mu\text{C}/\text{cm}^2$  for 1 wt. % excess PbO). This is understandable since 90% of the ceramic is textured at an angle to the polar direction.

### D. Piezoelectric properties of $\langle 001 \rangle$ -textured PMN-32.5PT ceramics from strain-field measurements

The unipolar strain-field behavior of the random PMN-32.5PT and PMN-32.5PT-5BT samples was collected by a

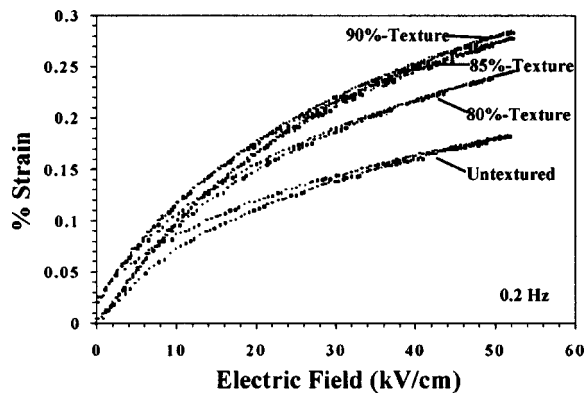


FIG. 7. Unipolar strain–electric field curves of PMN–32.5PT ceramics containing 5 vol % BaTiO<sub>3</sub> templates (PMN–32.5PT–5BT) displaying various degrees of texture.

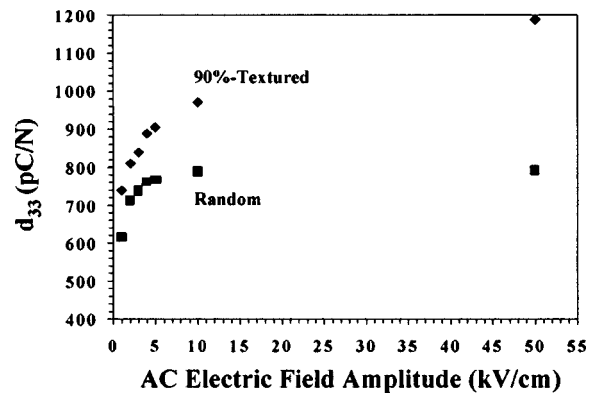


FIG. 8. Low-field (<5 kV/cm)  $d_{33}$  coefficients measured from unipolar strain–electric field curves of a ~90% textured PMN–32.5PT–5BT ceramic and a random PMN–32.5PT ceramic measured to maximum unipolar fields between 1 and 50 kV/cm.

linear variable differential transducer in conjunction with the Sawyer–Tower circuit (Fig. 7). The  $d_{33}$  coefficients were measured from the slope of the strain–field plots for fields both <5 and <10 kV/cm (Table I). The plot shows that increasing the (001)-texture increased the maximum strain output of the samples. The improvement in strain performance was enhanced up to an annealing time of 1–5 h, where it began to saturate along with the rate of texturing (Fig. 1). An untextured sample ( $f=0$ ) containing oriented BaTiO<sub>3</sub> templates showed a maximum strain of 0.161% at 50 kV/cm, and with ~90% texture ( $f=0.9$ ), the maximum strain increased to 0.279%. The low-field  $d_{33}$  coefficients (<5 kV/cm) for samples with ~90% texture ( $d_{33} \approx 1150$  pC/N) were 1.5 times greater than that measured for randomly oriented PMN–32.5PT samples containing 0 wt. % excess PbO (Table I). The  $d_{33}$  coefficients of this magnitude are approximately 40%–50% that measured for PMN–PT single crystals (30%–35% PbTiO<sub>3</sub>) in the (001).<sup>1,2,44,45</sup> The textured samples showed relatively little opening in the strain curves (0.0150%–0.0250%), but the hysteresis of the

textured samples, when correlated with the maximum opening in the strain–field curves, was greater than that measured for random PMN–32.5PT samples (Table I).

The degree of irreversible domain wall contribution to the piezoelectric coefficient is identified in strain–field plots by a large degree of piezoelectric hysteresis. Piezoelectric hysteresis can be defined as the difference in the strain–field response on the application and removal of the unipolar, electric field. The hysteresis is a result of domain wall motion due to nonstable domain configurations.<sup>46,47</sup> Rhombohedral single crystal PMN–PT poled and measured in the (001) show nearly anhysteretic strain–field response indicating the absence of extrinsic contribution due to the stable domain configuration.<sup>2</sup> The contribution of the domain motion to the piezoelectric response was further investigated in this work by observing the effect of various peak fields on the textured samples. A progressively increasing maximum field was applied to a ~90%-textured PMN–32.5PT–5BT sample from 1 to 50 kV/cm (0.2 Hz). Figure 8 shows the piezoelectric coefficient measured from the slope of the strain–field plot at

TABLE I. Piezoelectric properties measured from the strain–field plots for untextured and textured PMN–32.5PT ceramics containing various amounts of excess PbO and BaTiO<sub>3</sub> templates.

Sample	Texture fraction ( $f$ )	$d_{33}$ (pC/N) (<5 kV/cm)	$d_{33}$ (pC/N) (<10 kV/cm)	% Strain (50 kV/cm)	Max. opening in curve (%)
0 wt % PbO 0 vol % BT	Random	726	580	0.180	0.0180
1 wt % PbO 0 vol % BT	Random	721	593	0.177	0.0200
1 wt % PbO 5 vol % BT	0	590	500	0.161	0.0170
1 wt % PbO 5 vol % BT	0.80	975	808	0.235	0.0150
1 wt % PbO 5 vol % BT	0.85	990	820	0.240	0.0220
1 wt % PbO 5 vol % BT	0.90	1150	953	0.279	0.0239

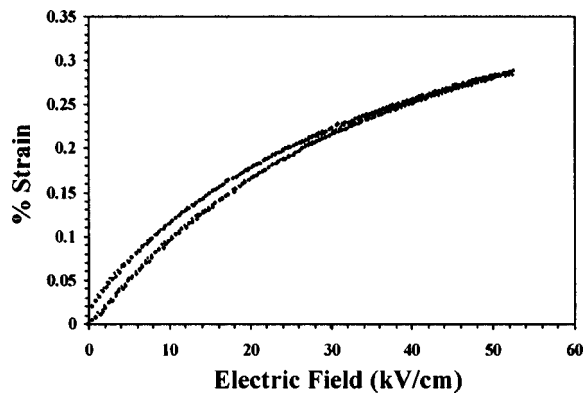


FIG. 9. Strain–electric field curves for a  $\sim 90\%$  textured PMN–32.5PT–5BT ceramic measured to a maximum field of 50 kV/cm after 1 and 50 000 cycles at 5 kV/cm. The strain–field response remained unchanged between 1 and 50 000 cycles.

fields  $< 5$  kV/cm at various maximum fields. At maximum applied fields  $< 5$  kV/cm ( $< E_c$ ), the slope of the plot ( $d_{33}$  coefficient) rapidly increased with an increase in maximum field. The rate of increasing slope and hysteresis began to subside at fields  $> 5$  kV/cm. A similar trend was observed for random PMN–32.5PT ceramics (0 wt. % excess PbO), but the slope and hysteresis quickly saturated at maximum applied fields  $> 5$  kV/cm. The random ceramic shows that the  $d_{33}$  coefficient is most strongly influenced by the hysteresis for ac drive fields greater than the coercive field ( $\sim 5$  kV/cm). This was not the case for the textured sample where the effective  $d_{33}$  coefficient continued to rise even at fields much greater than the coercive field.

There are several plausible reasons for the hysteresis in the textured samples. The splitting in the (200) XRD peaks shown in Fig. 2 suggested a possible presence of tetragonal domain states in the textured samples.<sup>19</sup> The presence of the tetragonal domain structure would increase the hysteresis. The origin of the hysteresis can also result from porosity ( $\sim 3\%$  in these experiments) or internal stresses developing during texturing, which would impede domain wall movement.<sup>35,36,48,49</sup> Internal stresses may result from the remnant BaTiO<sub>3</sub> templates embedded within the oriented grains. This could produce an internal stress field within the grains which might, for example, contribute to locally stabilizing the tetragonal PMN–PT.

In order to observe the longer term effect the domain movement has on the piezoelectric response, highly textured PMN–32.5PT–5BT samples ( $\sim 90\%$  texture) were driven in the  $\langle 001 \rangle$  through 50 000 cycles (5 Hz) at maximum unipolar field of 5 and 10 kV/cm. The intent of the piezoelectric degradation experiments was to identify the stability of the textured samples at various usable field levels. Comparing the initial high strain–field plot ( $< 50$  kV/cm) with the plot after 50 000 cycles at a maximum dc field of 5 kV/cm in Fig. 9, it can be seen that the general strain behavior remained consistent. By increasing the maximum applied voltage above the coercive field ( $\sim 10$  kV/cm), the textured material began to display progressive degradation (Fig. 10). A comparison of the initial and final (after 50 000 cycles) strain–field plot of the fatigued ceramic showed a large increase in the opening

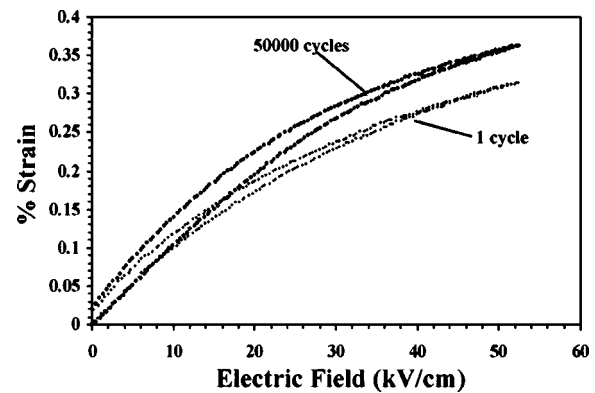


FIG. 10. Strain–electric field curves for a  $\sim 90\%$  textured PMN–32.5PT–5BT ceramic measured to a maximum field of 50 kV/cm after 50 000 cycles at 10 kV/cm.

of the strain–field response ( $> 0.04\%$ ) (Fig. 10). Again, the increase in hysteresis may be due to the activation of various domain walls above the coercive field or possibly heating, microcracking, or space-charge buildup.

The strain–field plots of the textured PMN–32.5PT ceramics did not show the field induced rhombohedral to tetragonal phase transformation ( $\sim 15$ – $30$  kV/cm) which is present in the  $\langle 001 \rangle$  single crystals.<sup>2,3,50</sup> The presence of the residual BaTiO<sub>3</sub> crystal within the templated grains may have affected the presence of this phase transformation by internally clamping the grains. This clamping would also restrict the piezoelectric response. The  $d_{33}$  and  $d_{31}$  coefficients for single crystal PMN–33PT ( $d_{33} \approx 2500$  pC/N,  $d_{31} \approx -1075$  pC/N)<sup>1,2,44,45</sup> are, respectively, 20–40 times greater than single crystal BaTiO<sub>3</sub> ( $d_{33} = 140$  pC/N,  $d_{31} = -34$ – $60$  pC/N).<sup>51</sup> Therefore, the BaTiO<sub>3</sub> core would restrict the expected strain of the PMN–PT grain.

There are a number of other factors that could affect and restrict the piezoelectric response of the textured samples produced in this work. The piezoelectric behavior would be affected by the intergranular PbO, orientation distribution, and residual porosity. The piezoelectric response may also be limited by the remaining randomly oriented matrix between the textured grains. The matrix grains could clamp the piezoelectric response between the templated grains. Lateral clamping may also arise due to the nature of the texture. A fiber-textured ceramic would not experience the same lateral response as a well-poled crystal. The random nature of the orientation perpendicular to the textured direction may complicate the polarization rotation responsible for the large single crystal strain. This lateral clamping of the textured grains would restrain the longitudinal response of the templated grains. Some of these variables must be further studied in order to understand the limiting factors and the full potential of these complicated textured materials.

#### E. Piezoelectric properties of $\langle 001 \rangle$ -textured PMN–32.5PT ceramics from resonance measurements

The piezoelectric coefficients ( $d_{33}, d_{31}$ ), mechanical compliances ( $s_{33}^E, s_{33}^D, s_{11}^E, s_{11}^D$ ), and the electromechanical coupling coefficients ( $k_{33}, k_{31}$ ) were also measured for the random PMN–32.5PT and textured PMN–32.5PT–5BT

TABLE II. Piezoelectric, electromechanical coupling, and compliance coefficients measured by the resonance technique for untextured and textured PMN–32.5PT ceramics containing various amounts of excess PbO and BaTiO<sub>3</sub> templates.

Sample	Texture fraction ( $f$ )	$d_{33}$ (pC/N)	$d_{31}$ (pC/N)	$k_{33}$	$k_{31}$	$(\times 10^{-12} \text{ m}^2/\text{N})$	$(\times 10^{-12} \text{ m}^2/\text{N})$
0 wt % PbO	Random	450	–211	0.719	0.403	17.7	12.5
0 vol % BT		$\pm 16$	$\pm 10$	$\pm 0.02$	$\pm 0.003$	$\pm 0.41$	$\pm 0.01$
1 wt % PbO	Random	376	–195	0.673	0.402	15.6	11.7
0 vol % BT		$\pm 6$	$\pm 8$	$\pm 0.002$	$\pm 0.001$	$\pm 0.05$	$\pm 0.05$
1 wt % PbO	0	370	–162	0.600	0.287	16.7	12.1
5 vol % BT		$\pm 1$	$\pm 6$	$\pm 0.006$	$\pm 0.007$	$\pm 0.4$	$\pm 0.9$
1 wt % PbO	0.80	518	–254	0.744	0.448	26.2	16.4
5 vol % BT		$\pm 10$	$\pm 22$	$\pm 0.007$	$\pm 0.020$	$\pm 1.0$	$\pm 0.7$
1 wt % PbO	0.90	525	–282	0.755	0.484	27.6	16.5
5 vol % BT		$\pm 35$	$\pm 18$	$\pm 0.006$	$\pm 0.007$	$\pm 1.7$	$\pm 0.14$

ceramic samples by the IEEE resonance technique.<sup>17</sup> The longitudinal coefficients were measured from samples which were cut to the dimensional ratio of 4:1:1 ( $4 \times 1 \times 1$  mm) and the lateral coefficients were obtained from samples with the dimensional ratio of 4:1:0.4 ( $4 \times 1 \times 0.4$  mm). The measured electromechanical coupling coefficients obtained for random PMN–32.5PT and PMN–32.5PT–5BT samples are shown in Table II. Randomly oriented PMN–32.5PT–5BT samples produced  $k_{33} \approx 0.60$ . This  $k_{33}$  coefficient is significantly below that observed for random PMN–32.5PT ceramics ( $k_{33} \approx 0.673$ ), indicating that the addition of the BaTiO<sub>3</sub> templates reduced the coupling coefficient of the samples. By increasing the texture fraction to  $\sim 0.90$ , the electromechanical coupling increased to  $k_{33} \approx 0.755$ . The resonance and antiresonance peaks of the textured samples showed some additional features, which may have originated from grain pullout or crack formation due to sample preparation, but the frequency of the minimum and maximum impedance were still reasonably well defined. These defects would have a significant effect on the resonance patterns, especially since the longitudinal resonance samples had a low number of textured grains, due to the large grain size ( $> 100 \mu\text{m}$ ), and a relatively small electrode area ( $\sim 1 \text{ mm}^2$ ).

The calculated lateral and longitudinal piezoelectric and compliance constants for random PMN–32.5PT and PMN–32.5PT–5BT samples are listed in Table II. The textured PMN–32.5PT–5BT samples generally showed slightly higher values than the random samples for all of the material constants. All of the constants increased with texturing. The compliances of the samples in the longitudinal and lateral directions showed greater anisotropy with additional texturing. The  $d_{33}/d_{31}$  ratio declined with texturing ( $\sim 2.35$ – $1.85$ ), but the average  $d_{33}/d_{31}$  ratio remained the same as the random PMN–32.5PT ceramics ( $\sim 2.1$ ). The  $d_{33}/d_{31}$  ratio typically found for many lead-based perovskite ferroelectric materials is  $\sim 2.32$ .<sup>7</sup> The discrepancy in the  $d_{33}/d_{31}$  ratio may originate from the difference in poling efficiency between the textured longitudinal and transverse resonance samples.

The  $d_{33}$  coefficients measured by the resonance technique for the highly textured PMN–32.5PT–5BT samples

were  $\sim 1.2$  times greater than that measured for randomly oriented PMN–32.5PT ceramics (0 wt. % excess PbO). A better comparison would be to associate the textured samples with the PMN–32.5PT composition containing 1 wt. % excess PbO. The  $d_{33}$  of the 90% textured sample was at least 1.4 times greater than its random ceramic counterpart. Therefore, the resonance measurements support the strain–field results indicating that fiber-texturing PMN–PT in the  $\langle 001 \rangle$  with a low volume fraction of BaTiO<sub>3</sub> templates increases the piezoelectric response. The difference in the degree of enhancement between the two measurement techniques may be the result of extrinsic contributions to the piezoelectric coefficients which were evident in the strain–field measurements.

In this work, the low-field piezoelectric coefficients measured by the low-field resonance technique for both the random and highly textured PMN–32.5PT ceramics were low. It is evident that the additions of the BaTiO<sub>3</sub> initially degraded the properties, but with an increase in the  $\langle 001 \rangle$  orientation fraction, the electromechanical coupling and compliance values increased, which resulted in an increase in the overall piezoelectric response. It was identified that the dielectric constant was not significantly altered with texturing, and the magnitude of the dielectric constant was primarily dominated by the intergranular PbO-based phase. Therefore, the calculated piezoelectric coefficients were dictated by the low dielectric constant of the textured PMN–32.5PT ceramics ( $\epsilon_{33}^T < 3000$ ).

The important detail identified in this work was that the textured samples consistently displayed strains, piezoelectric coefficients, electromechanical coupling coefficients, and compliances greater than its randomly oriented counterpart. This comparison was based on random ceramic standards which were synthesized with the same materials and measured with the same techniques as the textured ceramics. It also suggests that additional property improvements could be expected as the second phase or residual misoriented material are eliminated, and by better matching the dielectric and electromechanical properties of the template to the matrix.

#### IV. CONCLUSIONS

PMN-32.5PT ceramics were fiber textured in the  $\langle 001 \rangle$  by the TGG process using  $\{001\}$ -BaTiO<sub>3</sub> template particles and 1 wt. % excess PbO. With an increase in texture, the PMN-32.5PT ceramic samples showed increased piezoelectric, electromechanical coupling, and compliance coefficients. The  $d_{33}$  piezoelectric coefficients of highly textured PMN-32.5PT ceramics were 1.2–1.5 times greater than randomly oriented samples. The enhancement in the electromechanical response was limited by their relatively lower dielectric constant ( $\epsilon_{33}^T < 3000$ ) due to the presence of the residual intergranular PbO phase, which was intentionally added to enhance the texturing kinetics. The strain–field response of the textured samples showed piezoelectric hysteresis when measured in the textured direction. This differs from the behavior identified for domain engineered PMN-32PT single crystals which show little to no piezoelectric hysteresis in the  $\langle 001 \rangle$ . The hysteresis suggests some extrinsic contribution to the piezoelectric coefficient of the textured samples. Partial clamping by the residual intragranular BaTiO<sub>3</sub> template particles was identified to limit the mobility of the domain walls. Mechanical clamping by unoriented/misoriented grains, intergranular PbO, and porosity may also limit the poling efficiency and the polarization rotation.

#### ACKNOWLEDGMENTS

The authors would like to acknowledge the financial support from a subcontract under Materials Systems Inc., Littleton, MA, under DARPA/NAVSEA Contract No. N66604-99-C-4622 and DARPA Grant No. F49620-00-1-0098. The authors would also like to thank Tim Klinger, Jeff Long, and Paul Moses for their invaluable technical support.

- <sup>1</sup>S.-E. Park and T. R. Shrout, IEEE Trans. Ultrason. Ferroelectr. Freq. Control **44**, 140 (1997).
- <sup>2</sup>S.-E. Park and T. R. Shrout, J. Appl. Phys. **82**, 1804 (1997).
- <sup>3</sup>J. Yin and W. Cao, J. Appl. Phys. **87**, 7438 (2000).
- <sup>4</sup>S.-E. Park, S. Wada, L. E. Cross, and T. R. Shrout, J. Appl. Phys. **86**, 2746 (1999).
- <sup>5</sup>P. W. Rehrig, S.-E. Park, S. Trolier-McKinstry, G. L. Messing, B. Jones, and T. R. Shrout, J. Appl. Phys. **86**, 1657 (1999).
- <sup>6</sup>J.-P. Maria, W. Hackenberger, and S. Trolier-McKinstry, J. Appl. Phys. **84**, 5147 (1998).
- <sup>7</sup>J. H. Park, F. Xu, and S. Trolier-McKinstry, J. Appl. Phys. **89**, 568 (2001).
- <sup>8</sup>C. Duran, S. Trolier-McKinstry, and G. L. Messing, J. Am. Ceram. Soc. **83**, 2203 (2000).
- <sup>9</sup>K. Nagata and K. Okazaki, Jpn. J. Appl. Phys., Part 1 **24**, 812 (1985).
- <sup>10</sup>J. A. Horn, S. C. Zhang, U. Selvaraj, G. L. Messing, and S. Trolier-McKinstry, J. Am. Ceram. Soc. **82**, 921 (1999).
- <sup>11</sup>S.-H. Hong, S. Trolier-McKinstry, and G. L. Messing, J. Am. Ceram. Soc. **83**, 113 (2000).
- <sup>12</sup>E. M. Sabolsky, A. R. James, S. Kwon, S. Trolier-McKinstry, and G. L. Messing, Appl. Phys. Lett. **78**, 2551 (2001).
- <sup>13</sup>B. Brahmarouti, Ph.D. thesis, Pennsylvania State University, 1999.
- <sup>14</sup>M. M. Seabaugh, I. H. Kerscht, and G. L. Messing, J. Am. Ceram. Soc. **80**, 1181 (1997).

- <sup>15</sup>J. P. Remeika, J. Am. Chem. Soc. **76**, 940 (1954).
- <sup>16</sup>F. K. Lotgering, J. Inorg. Nucl. Chem. **9**, 113 (1959).
- <sup>17</sup>The Institute of Electrical and Electronics Engineers, Inc., An American National Standard, IEEE Standard on Piezoelectricity, ANSI/IEEE Std. 176-1987, New York, 1988.
- <sup>18</sup>E. M. Sabolsky, S. Trolier-McKinstry, and G. L. Messing, J. Am. Ceram. Soc. **84**, 2507 (2001).
- <sup>19</sup>M. K. Durbin, J. C. Hicks, S.-E. Park, and T. R. Shrout, J. Appl. Phys. **87**, 8159 (2000).
- <sup>20</sup>S. L. Swartz, T. R. Shrout, W. A. Schulze, and L. E. Cross, J. Am. Ceram. Soc. **67**, 311 (1984).
- <sup>21</sup>J. Chen and M. P. Harmer, J. Am. Ceram. Soc. **73**, 68 (1990).
- <sup>22</sup>H. C. Ling, A. M. Jackson, M. F. Yan, and W. W. Rhodes, J. Mater. Res. **5**, 629 (1990).
- <sup>23</sup>H.-C. Wang and W. A. Schulze, J. Am. Ceram. Soc. **73**, 825 (1990).
- <sup>24</sup>M. Villegas, A. C. Caballero, M. Kosec, C. Moure, P. Duran, and J. F. Fernandez, J. Mater. Res. **14**, 891 (1999).
- <sup>25</sup>M. H. Frey, Z. Xu, P. Han, and D. A. Payne, Ferroelectrics **206/207**, 337 (1998).
- <sup>26</sup>P. Papet, J. P. Dougherty, and T. R. Shrout, J. Mater. Res. **12**, 2902 (1990).
- <sup>27</sup>C. A. Randall, A. D. Hilton, D. J. Barber, and T. R. Shrout, J. Mater. Res. **8**, 880 (1993).
- <sup>28</sup>R. A. Fry, M. S. thesis, The Pennsylvania State University, 1992.
- <sup>29</sup>S. W. Choi, T. R. Shrout, S. J. Jang, and A. S. Bhalla, Mater. Lett. **8**, 253 (1989).
- <sup>30</sup>S. W. Choi, T. R. Shrout, S. J. Jang, and A. S. Bhalla, Ferroelectrics **100**, 29 (1989).
- <sup>31</sup>J. Zhao, Q. M. Zhang, N. Kim, and T. Shrout, Jpn. J. Appl. Phys., Part 1 **34**, 5658 (1995).
- <sup>32</sup>A. D. Hilton, C. A. Randall, D. J. Barber, and T. R. Shrout, Ferroelectrics **93**, 379 (1989).
- <sup>33</sup>J. Kelly, M. Leonard, C. Tantigate, and A. Safari, J. Am. Ceram. Soc. **80**, 957 (1997).
- <sup>34</sup>X. Zhang and F. Fang, J. Mater. Res. **14**, 4581 (1999).
- <sup>35</sup>K. Okazaki and K. Nagata, J. Am. Ceram. Soc. **56**, 82 (1973).
- <sup>36</sup>M. Kiyohara, K. Katoh, and K. Nagata, J. Ceram. Soc. Jpn. **104**, 201 (1996).
- <sup>37</sup>S.-Y. Chen, S.-Y. Cheng, and S.-M. Wang, J. Am. Ceram. Soc. **74**, 400 (1991).
- <sup>38</sup>Y. S. Cho, S. M. Pilgrim, H. Giesche, and K. Bridger, J. Am. Ceram. Soc. **83**, 2473 (2000).
- <sup>39</sup>O. Sakurai, M. Katsumoto, K. Shinozaki, and N. Mizutani, J. Ceram. Soc. Jpn. **101**, 594 (1993).
- <sup>40</sup>A. Halliyal, U. Kumar, R. E. Newnham, and L. E. Cross, Am. Ceram. Soc. Bull. **66**, 671 (1987).
- <sup>41</sup>J. R. Belsick, A. Halliyal, U. Kumar, and R. E. Newnham, Am. Ceram. Soc. Bull. **66**, 664 (1987).
- <sup>42</sup>F. Chu, I. M. Reaney, and N. Setter, J. Appl. Phys. **77**, 1671 (1995).
- <sup>43</sup>B.-Y. Ahn and N.-K. Kim, J. Am. Ceram. Soc. **83**, 1720 (2000).
- <sup>44</sup>W. Cao, Associate Professor of Mathematics and Materials Science, Penn State University (personal communication, 2001).
- <sup>45</sup>T. R. Shrout, Z. P. Chang, N. Kim, and S. Markgraf, Ferroelectr. Lett. Sect. **12**, 63 (1990).
- <sup>46</sup>S. Li, W. Cao, and L. E. Cross, J. Appl. Phys. **69**, 7219 (1991).
- <sup>47</sup>Q. M. Zhang, H. Wang, N. Kim, and L. E. Cross, J. Appl. Phys. **75**, 454 (1994).
- <sup>48</sup>S. C. Hwang and G. Arlt, J. Appl. Phys. **87**, 869 (2000).
- <sup>49</sup>F. Xu, S. Trolier-McKinstry, W. Ren, B. Xu, Z.-L. Xie, and K. J. Hemker, J. Appl. Phys. **89**, 1336 (2001).
- <sup>50</sup>D.-S. Paik, S.-E. Park, S. Wada, S.-F. Liu, and T. R. Shrout, J. Appl. Phys. **85**, 1080 (1999).
- <sup>51</sup>N. A. Pertsev, A. G. Zembilgotov, and R. Waser, J. Appl. Phys. **84**, 1524 (1998).